Journal of Marine Science and Application (2026) 25: 630-639
https://doi.org/10.1007/s11804-025-00694-5

RESEARCH ARTICLE

Turbo Equalization for Time-Varying Underwater Acoustic Channels with Imperfect Channel State Information

Jiaheng Zhang[1,2,3], Wei Ge[1,2,3,4], Wentao Tong[1,2,3] and Lin Cheng[1,2,3]

Received: 18 January 2025 / Accepted: 10 March 2025

Abstract

Turbo equalization is commonly employed to compensate for multipath propagation in underwater acoustic (UWA) communication. However, the performance of turbo equalization degrades due to the imperfect channel state information (CSI) and time-varying channels. Herein, we first introduce a new derivation for turbo equalization based on the joint Gaussian criterion. On the basis of this derivation, a novel turbo equalization algorithm for time-varying UWA channels with imperfect CSI is proposed. The algorithm combines the imperfect CSI with the temporal coherence characteristics of UWA channels, which are modeled as a first-order autoregressive (AR(1)) process, to achieve a more accurate channel *a posteriori* distribution. Afterward, the refined distribution is incorporated into the design of the turbo equalizer, which can effectively reduce intersymbol interference and the Doppler effect. Simulation results show that the proposed algorithm has a better bit error rate performance than other turbo equalization algorithms with channel estimation error compensation or the AR(1) process for any iteration in fast time-varying scenarios.

Keywords Imperfect channel state information; First-order autoregressive process; Turbo equalization; Time-varying channels; Underwater acoustics communication

1 Introduction

Underwater acoustic (UWA) communication is a relatively common communication scenario, which is often affected by the Doppler effect and multipath propagation in UWA channels (Ge et al., 2024; Sun et al., 2023; Liu et al., 2023; Yin et al., 2024). Multipath propagation can lead to intersymbol interference (ISI) (Naman and Abdelkareem, 2023). Conventional turbo equalizers use iterative soft-input soft-output (SISO) equalization and decoding to mitigate ISI under the assumption of time-invariant channel and perfect knowledge of channel state information (CSI) (Tüchler et al., 2002; Zheng et al., 2015). The Doppler effect can lead to inaccuracies in channel estimation, thereby causing errors in the calculation of equalization coefficients (Abdelkareem et al., 2011; Abdelkareem et al., 2016). To compensate for the Doppler effect caused by time-varying UWA channels, utilizing estimated symbols for channel tracking is a common method during turbo iteration. Time-varying UWA channels were estimated by Zhang et al. (2018) by solving the recursive least squares (LS) normal equation, which is established by the symbol *a priori* information from the turbo decoder. Assuming that the UWA channel follows a first-order autoregressive (AR(1)) process is also a common modeling approach, where the current channel state is influenced by the previous channel state and estimation noise. A joint bidirectional channel estimation (BCE) and turbo equalization algorithm was proposed by Yang et al. (2021), which assumed that the UWA channels satisfied the AR(1) process at different moments and used the superimposed pilot symbols from the turbo decoder to re-estimate the UWA

Article Highlights

- The assumption that the channel state information is perfectly known to the receiver does not hold in practical UWA communication.
- We proposed a novel turbo equalization algorithm considering the imperfect CSI and the AR(1) process.
- We use data-aided channel re-estimation to track the UWA channels and then update the re-estimated channel's *a posteriori* distribution.
- Simulation results show that the proposed algorithm outperforms other methods in fast time-varying scenarios.

✉ Wei Ge
gewei@hrbeu.edu.cn

[1] National Key Laboratory of Underwater Acoustic Technology, Harbin Engineering University, Harbin 150001, China

[2] Key Laboratory for Polar Acoustics and Application of Ministry of Education (Harbin Engineering University), Ministry of Education, Harbin 150001, China

[3] College of Underwater Acoustic Engineering, Harbin Engineering University, Harbin 150001, China

[4] State Key Laboratory of Acoustics, Institute of Acoustics, Chinese Academy of Science, Beijing 10090, China

channel. The AR(1) model was combined with the Bayesian framework for channel estimation, which was applied to turbo equalization (Liang et al., 2023). A turbo equalization method was proposed with the joint symbol, channel, and impulse noise estimation based on the AR(1) model (Zhang et al., 2024). These turbo equalizers all assume that the CSI is perfectly known to the receiver. However, this assumption does not hold in practical UWA communication, leading to channel estimation error (CEE), which degrades the bit error rate (BER) performance of the equalizer.

LS estimation (LSE) is widely used in UWA channel estimation because it is simple and does not require channel statistics (Zhang et al., 2022). The combination of LSE and superimposed training by Yang et al. (2022) can track time-varying channels. LSE was utilized by Jiang and Diamant (2023) as a coarse estimate to distinguish the sparsity of UWA channels. However, LSE ignores the sparsity of UWA channels, resulting in considerable CEE compared to compressive sensing methods (Khan et al., 2020; Guo et al., 2021). In our simulation, the BER performance of LSE is considerably inferior to that of sparse Bayesian learning (SBL) channel estimation.

Imperfect CSI refers to a situation where receivers do not perfectly know the CSI and can only obtain the channel estimate, which will be impacted by CEE. There has been extensive research on imperfect CSI in terrestrial radio frequency (RF) communication systems. Li et al. (2016) and Jiang et al. (2018) demonstrated the impact of CEE caused by LSE and proposed turbo equalizers with CEE compensation, resulting in remarkable ISI mitigation, particularly under low signal-to-noise ratio (SNR) conditions. Robust turbo equalizers were proposed by Zhu et al. (2016) and Zhe et al. (2018), which utilized the statistical properties of CEE. To compensate for the CEE due to time-varying channels, closely relevant studies (Fodor et al., 2021; Fodor et al., 2023) considered the memory characteristics of Rayleigh channels and proposed a linear receiver with imperfect CSI that minimizes the mean squared error (MSE). The core idea of utilizing imperfect CSI is to use the channel *a priori* distribution and statistical properties of the coarse channel estimation to form a more accurate channel *a posteriori* distribution, which can bring considerable performance gains.

Compared to those in RF wireless channels, the multipath propagation and Doppler effect in UWA channels are more severe because the speed of sound is much lower than the speed of light (Yin et al., 2019). The multipath structure of UWA channels is more complex, and the channel structure varies within tens or hundreds of symbol durations (Roudsari et al., 2017; Zhang et al., 2019). In this scenario, compensating for CEEs caused by LSE is necessary, and the linear receiver proposed by Fodor et al. (2021) may not be optimal. However, to our knowledge, there is little literature utilizing imperfect CSI in UWA communication. Therefore, inspired by the time-varying channel model proposed by Fodor et al. (2021), we aim to use estimated channels at different moments to obtain a channel *a posteriori* distribution and incorporate it into the design of the turbo equalizer. The contributions of this article can be summarized as follows.

- We give a new derivation for turbo equalization based on the joint Gaussian (JG) criterion, which is equivalent to the turbo equalizer proposed by Yuan et al. (2008) and Guo et al. (2009).
- On the basis of this derivation, we derive the channel *a posteriori* distribution in fast time-varying scenarios utilizing the AR(1) process and imperfect CSI, which is incorporated into the design of the turbo equalizer. Simulation results show that the proposed algorithm provides a better BER performance than other methods.

This paper is organized as follows. Section 2 provides a new derivation for turbo equalization and describes the UWA channel *a posteriori* distribution. Section 3 details the proposed turbo equalization for time-varying UWA channels with imperfect CSI. Section 4 shows the simulation results. Section 5 analyzes the computational complexity of the conventional and proposed algorithms. Finally, Section 6 concludes this paper.

Notations: The superscripts $(\cdot)^*$, $(\cdot)^{\mathrm{T}}$, $(\cdot)^{\mathrm{H}}$, and $(\cdot)^{\dagger}$ represent conjugate, transpose, conjugate transpose, and pseudo-inverse, respectively. $\boldsymbol{I}_N$ denotes the $N \times N$ identity matrix. $\mathbb{E}_{\boldsymbol{x}}(\boldsymbol{y})$ and $\mathrm{Cov}_{\boldsymbol{x}}(\boldsymbol{y},\boldsymbol{y})$ represent the expectation and covariance matrix of a random variable $\boldsymbol{y}$ with respect to $\boldsymbol{x}$, respectively.

2 Turbo equalization and channel estimation

2.1 New derivation for turbo equalization

First, we introduce a new derivation for turbo equalization based on the JG criterion. We consider a widely used UWA communication system that uses single-carrier (SC) block transmission with a cyclic prefix (CP). The insertion of CP can simplify the derivation as the channel matrix is a square matrix. The derivation is performed in the time domain without loss of generality. SC modulation has a lower peak-to-average power ratio and is less sensitive to carrier frequency offset than orthogonal frequency-division multiplexing modulation (Tao, 2015). The signal block structure is shown in Figure 1, with pilot and data (including the CP) lengths of P and N, respectively. The pilot sequences at the beginning and end are used for channel estimations at two moments (denoted $t-1$ and t). We assume that the UWA channel is time-invariant within time slots t and $(t-1)$ rather than within a symbol duration. The transmitted symbols $\{x_n\}_{n=0}^{N-1}$ modulated by M-ary phase-shift keying (PSK) correspond to the encoded and interleaved bits $\{c_{n,j}\}_{j=0}^{M-1}$.

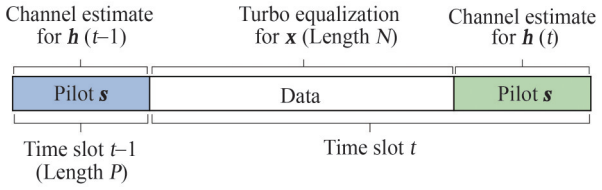

Figure 1 Signal block structure

The bits are mapped to $\{x_n\}$ according to the M-ary PSK–modulated symbols $\{\chi_i\}_{i=0}^{2^M-1}$, where χ_i corresponds to the bits $\{q_{i,j}\}_{j=0}^{M-1}$. At moment t, assuming that the length of the UWA channel $\boldsymbol{h}(t)$ is L, the received signal $\boldsymbol{y}$ from the hydrophone is

$$\boldsymbol{y} = \boldsymbol{H}(t)\boldsymbol{x} + \boldsymbol{w}(t) \tag{1}$$

where $\boldsymbol{H}(t) \in \mathbb{C}^{N\times N}$ is a circulant matrix with the first column being $\left[\boldsymbol{h}(t)^{\mathrm{T}}, 0, \cdots, 0\right]^{\mathrm{T}}$ and $\boldsymbol{w}(t)$ is additive white Gaussian noise with zero mean and covariance $\sigma_\omega^2 \boldsymbol{I}_N$. The detailed modeling of UWA channels can be found in the study by Naman and Abdelkareem (2023).

According to Eq. (1), the *a posteriori* mean and covariance of $\boldsymbol{y}$ with the JG distribution conditioned on bit $c_{n,j}$ are

$$\begin{aligned}\boldsymbol{\mu} &\triangleq \mathbb{E}_{\boldsymbol{x},\boldsymbol{w}}\left(\boldsymbol{y}\middle|c_{n,j}\right)\\ &= \boldsymbol{H}(t)\mathbb{E}(\boldsymbol{x}) - \boldsymbol{h}_n(t)\mathbb{E}\left(x_n\right) + \chi_{q_{i,j}=c_{n,j}}\boldsymbol{h}_n(t)\end{aligned} \tag{2}$$

$$\begin{aligned}\boldsymbol{\Sigma} &\triangleq \mathrm{Cov}_{\boldsymbol{x},\boldsymbol{w}}\left(\boldsymbol{y},\boldsymbol{y}\middle|c_{n,j}\right)\\ &= v\boldsymbol{H}(t)\boldsymbol{H}(t)^{\mathrm{H}} + \sigma_\omega^2\boldsymbol{I}_N - v\boldsymbol{h}_n(t)\boldsymbol{h}_n(t)^{\mathrm{H}}\end{aligned} \tag{3}$$

where $\chi_{q_{i,j}=c_{n,j}}$ is the mapped symbol χ_i that satisfies $q_{i,j} = c_{n,j}$, and $\boldsymbol{h}_n(t)$ is the nth row of $\boldsymbol{H}(t)$. $\mathbb{E}(x_n)$ and v are the *a priori* mean and variance of x_n, respectively. The variance v can be approximated from $\mathrm{Cov}(\boldsymbol{x},\boldsymbol{x}) \approx v\boldsymbol{I}_N$ (Guo et al., 2009).

The output log-likelihood ratio (LLR) of the SISO equalizer is

$$\lambda_{n,j} = \ln\frac{\sum\limits_{\forall\chi_i: q_{i,j}=0} p\left(\boldsymbol{y}|c_{n,j}=0\right)\prod\limits_{j'\neq j}P\left(c_{n,j'}=q_{i,j'}\right)}{\sum\limits_{\forall\chi_i: q_{i,j}=1} p\left(\boldsymbol{y}|c_{n,j}=1\right)\prod\limits_{j'\neq j}P\left(c_{n,j'}=q_{i,j'}\right)} \tag{4}$$

The exponential term of $p\left(\boldsymbol{y}\middle|c_{n,j}\right)$ can be simplified as

$$\left(\boldsymbol{y}-\boldsymbol{\mu}\right)^{\mathrm{H}}\boldsymbol{\Sigma}\left(\boldsymbol{y}-\boldsymbol{\mu}\right) = \mathrm{Const} - 2\mathrm{Re}\left\{\left(\chi_{q_{i,j}=c_{n,j}}\right)^{*}\boldsymbol{h}_n(t)^{\mathrm{H}}\boldsymbol{\Sigma}^{-1}\boldsymbol{A}\right\} \tag{5}$$

where $\boldsymbol{A} = \boldsymbol{y} - \boldsymbol{H}(t)\mathbb{E}(\boldsymbol{x}) + \boldsymbol{h}_n(t)\mathbb{E}(x_n)$. By substituting Eqs. (2), (3), and (5) into Eq. (4), we have

$$\lambda_{n,j} = \ln\frac{\sum\limits_{\forall\chi_i: q_{i,j}=0}\exp\left(\mathrm{Re}\left\{\left(\chi_{q_{i,j}=0}\right)^{*}\boldsymbol{h}_n(t)^{\mathrm{H}}\boldsymbol{\Sigma}^{-1}\boldsymbol{A}\right\} + \frac{1}{2}\sum\limits_{j\neq j'}\tilde{q}_{i,j'}\gamma_{n,j'}\right)}{\sum\limits_{\forall\chi_i: q_{i,j}=1}\exp\left(\mathrm{Re}\left\{\left(\chi_{q_{i,j}=1}\right)^{*}\boldsymbol{h}_n(t)^{\mathrm{H}}\boldsymbol{\Sigma}^{-1}\boldsymbol{A}\right\} + \frac{1}{2}\sum\limits_{j\neq j'}\tilde{q}_{i,j'}\gamma_{n,j'}\right)} \tag{6}$$

where $\gamma_{n,j}$ is the *a priori* LLR of $c_{n,j}$ from the SISO decoder and $\tilde{q}_{i,j}$ satisfies

$$\tilde{q}_{i,j} = \begin{cases}+1, & q_{i,j}=0\\ -1, & q_{i,j}=1\end{cases} \tag{7}$$

We set $\beta = \boldsymbol{h}_n(t)^{\mathrm{H}}\boldsymbol{\Sigma}^{-1}\boldsymbol{A}$. Specifically, for quadrature PSK (QPSK)–modulated symbols

$$\{\chi_i\}_{i=0}^{3} = \frac{1}{\sqrt{2}}\{1+j, -1+j, -1-j, 1-j\} \tag{8}$$

When $j = 0$, Eq. (4) can be written as

$$\begin{aligned}\lambda_{n,0} &= \ln\frac{\exp\left\{\mathrm{Re}\left\{\chi_0^{*}\beta\right\} + \gamma_{n,1}/2\right\} + \exp\left\{\mathrm{Re}\left\{\chi_3^{*}\beta\right\} - \gamma_{n,1}/2\right\}}{\exp\left\{\mathrm{Re}\left\{\chi_1^{*}\beta\right\} + \gamma_{n,1}/2\right\} + \exp\left\{\mathrm{Re}\left\{\chi_2^{*}\beta\right\} - \gamma_{n,1}/2\right\}}\\ &= \ln\frac{K_0\cdot\exp\left\{\sqrt{2}\,\mathrm{Re}\left\{\beta\right\}\right\}}{K_0\cdot\exp\left\{-\sqrt{2}\,\mathrm{Re}\left\{\beta\right\}\right\}} = 2\sqrt{2}\,\mathrm{Re}\left\{\boldsymbol{h}_n(t)^{\mathrm{H}}\boldsymbol{\Sigma}^{-1}\boldsymbol{A}\right\}\end{aligned} \tag{9}$$

where

$$K_0 = \cos\left(\mathrm{Im}\left\{\boldsymbol{h}_n^{\mathrm{H}}\boldsymbol{\Sigma}^{-1}\boldsymbol{A}\right\}/\sqrt{2} + \gamma_{n,j'}/2\right) \tag{10}$$

Similarly, $\lambda_{n,1}$ can be derived as

$$\lambda_{n,1} = 2\sqrt{2}\,\mathrm{Im}\left\{\boldsymbol{h}_n(t)^{\mathrm{H}}\boldsymbol{\Sigma}^{-1}\boldsymbol{A}\right\} \tag{11}$$

The turbo equalizer obtained from Eq. (6) is equivalent to the turbo equalizer proposed by Yuan et al. (2008) and Guo et al. (2009). For binary PSK (BPSK) modulation, because the mapping between symbols and bits is surjective, Eq. (6) can be written as

$$\lambda_{n,0} = \ln\frac{p\left(\boldsymbol{y}\middle|c_{n,0}=0\right)}{p\left(\boldsymbol{y}\middle|c_{n,0}=1\right)} = \ln\frac{p\left(\boldsymbol{y}\middle|x_n=+1\right)}{p\left(\boldsymbol{y}\middle|x_n=-1\right)} \tag{12}$$

which is consistent with Eq. (2) in Yuan et al. (2008). For QPSK modulation, Eqs. (9) and (11) are the real and imaginary parts of Eq. (8a) in Guo et al. (2009), and they differ by $\sqrt{2}$ times. This is because it converts the transmitted and received complex vectors into real vectors, which can be regarded as BPSK-modulated symbols, and computes the LLRs using Eq. (12).

2.2 Channel estimation

Let the pilot sequence be $\boldsymbol{s} = \left[s_0, s_1, \cdots, s_{P-1}\right]^{\mathrm{T}}$. The pilot signal $\boldsymbol{y}_{\mathrm{pilot}}(t)$ received from the hydrophone is

$$\boldsymbol{y}_{\mathrm{pilot}}(t) = \boldsymbol{S}\boldsymbol{h}(t) + \boldsymbol{w}(t) \tag{13}$$

where the dictionary matrix $\boldsymbol{S}$ is a Toeplitz matrix, which is composed as

$$\boldsymbol{S} = \begin{bmatrix} s_{L-1} & s_{L-2} & \cdots & s_0 \\ s_L & s_{L-1} & \cdots & s_1 \\ \vdots & & & \vdots \\ s_{P-1} & s_{P-2} & \cdots & s_{P-L+1} \end{bmatrix} \in \mathbb{C}^{(P-L+1)\times L} \tag{14}$$

The LSE of the UWA channel at the t moment can be written as

$$\hat{\boldsymbol{h}}(t) = (\boldsymbol{S})^{\dagger}\boldsymbol{y}_{\mathrm{pilot}} = \boldsymbol{h}(t) + \underbrace{(\boldsymbol{S})^{\dagger}\boldsymbol{w}(t)}_{\text{Channel Estimation Error}} \tag{15}$$

We assume that the *a priori* distribution of the UWA channel follows $\boldsymbol{h}(t) \sim \mathcal{CN}(\boldsymbol{0}, \boldsymbol{I}_L)$. Therefore, the distribution of the estimated channel $\hat{\boldsymbol{h}}(t)$ satisfies

$$\hat{\boldsymbol{h}}(t) \sim \mathcal{CN}(\boldsymbol{0}, \underbrace{\boldsymbol{I}_L + \sigma_{\omega}^2(\boldsymbol{S}^{\mathrm{H}}\boldsymbol{S})^{-1}}_{\triangleq \boldsymbol{R}}) \tag{16}$$

As the pilot sequences are the same at two moments, $\hat{\boldsymbol{h}}(t-1)$ also satisfies Eq. (16).

Given the LS-estimated channels $\hat{\boldsymbol{h}}(t)$ and $\hat{\boldsymbol{h}}(t-1)$, the *a posteriori* distribution of $\boldsymbol{h}(t)$ satisfies

$$\left(\boldsymbol{h}(t) \,\middle|\, \hat{\boldsymbol{h}}(t), \hat{\boldsymbol{h}}(t-1)\right) \sim \boldsymbol{E}\boldsymbol{\zeta}(t) + \mathcal{CN}(\boldsymbol{0}, \boldsymbol{Z}) \tag{17}$$

where

$$\boldsymbol{\zeta}(t) = \begin{bmatrix} \hat{\boldsymbol{h}}(t) \\ \hat{\boldsymbol{h}}(t-1) \end{bmatrix} \tag{18}$$

$$\boldsymbol{E} = \begin{bmatrix} \boldsymbol{I}_L & \alpha\boldsymbol{I}_L \end{bmatrix} \begin{bmatrix} \boldsymbol{R} & \alpha\boldsymbol{I}_L \\ \alpha\boldsymbol{I}_L & \boldsymbol{R} \end{bmatrix}^{-1} \tag{19}$$

$$\boldsymbol{Z} = \boldsymbol{I}_L - \boldsymbol{E}\begin{bmatrix} \boldsymbol{I}_L \\ \alpha\boldsymbol{I}_L \end{bmatrix} \tag{20}$$

and $\boldsymbol{h}(t) \sim \mathcal{CN}(\boldsymbol{0}, \boldsymbol{I}_L)$, with $\boldsymbol{R} = \boldsymbol{I}_L + \sigma_{\omega}^2(\boldsymbol{S}^{\mathrm{H}}\boldsymbol{S})^{-1}$ being the covariance of $\hat{\boldsymbol{h}}(t)$ and α being the channel correlation coefficient in the AR(1) process. The proof is in Appendix II in Fodor et al. (2021).

The SISO equalization coefficients can be obtained according to the channel *a posteriori* distribution. It is noted that we utilize LS channel estimation in this article, while other methods, such as MMSE and Kalman channel estimation, can also be used to compute the distribution as above (Zhe et al., 2018; Fodor et al., 2021).

3 Proposed turbo equalization for time-varying UWA channels

This section derives a turbo equalizer for time-varying UWA channels based on the JG criterion. The structure of the turbo equalizer shown in Figure 2 is mainly divided into three parts.

- **SISO equalization**. On the basis of the channel *a posteriori* distribution obtained from the observations at two moments, the SISO equalization coefficients are computed.
- **Data-aided channel re-estimation**. The channels at two moments are re-estimated using soft decision symbols. The re-estimated channels are then combined with the previously estimated channels to obtain the channel estimation with minimum Bayesian MSE (BMSE).
- ***A posteriori* distribution update**. The channel *a posteriori* distribution is updated according to the re-estimated channels, and the SISO equalization coefficients are recomputed based on the updated distribution.

3.1 SISO equalization conditioned on channel estimation

We assume that the UWA channel, the transmitted acoustic signal, and the noise are uncorrelated. Considering the impact of imperfect CSI on the received signal, the mean of $\boldsymbol{y}$ conditioned on the channel estimates $\hat{\boldsymbol{h}}^{(i)}(t)$ and $\hat{\boldsymbol{h}}^{(i)}(t-1)$ in the ith iteration is

$$\begin{aligned} &\mathbb{E}_{\boldsymbol{x},\boldsymbol{w},\boldsymbol{h}(t)}\left(\boldsymbol{y} \,\middle|\, c_{n,j}, \hat{\boldsymbol{h}}^{(i)}(t), \hat{\boldsymbol{h}}^{(i)}(t-1)\right) \\ &\quad = \tilde{\boldsymbol{H}}\mathbb{E}^{(i)}(\boldsymbol{x}) - \tilde{\boldsymbol{h}}_n\mathbb{E}^{(i)}(x_n) + \chi_{q_{i,j}=c_{n,j}}\tilde{\boldsymbol{h}}_n \end{aligned} \tag{21}$$

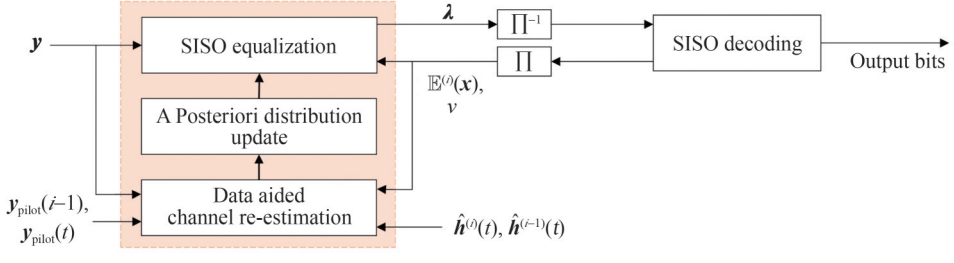

Figure 2 Structure of the proposed turbo equalizer. Π and Π^{-1} denote interleaving and deinterleaving, respectively

where $\tilde{\boldsymbol{H}} \in \mathbb{C}^{N\times N}$ is a circulant matrix with the first column being $\left[\left(\boldsymbol{E}^{(i)}\boldsymbol{\zeta}^{(i)}(t)\right)^{\mathrm{T}}, 0, \cdots, 0\right]^{\mathrm{T}}$ and $\tilde{\boldsymbol{h}}_n$ is the nth column of $\tilde{\boldsymbol{H}}$.

Because $\boldsymbol{H}(t)\boldsymbol{H}(t)^{\mathrm{H}} = \sum_{k=0}^{N-1}\boldsymbol{h}_k(t)\boldsymbol{h}_k(t)^{\mathrm{H}}$, the covariance of $\boldsymbol{y}$ conditioned on the estimated channels is

$$\begin{aligned}\tilde{\boldsymbol{\Sigma}} &\triangleq \mathrm{Cov}_{\boldsymbol{x},\boldsymbol{w},\boldsymbol{h}(t)}\left(\boldsymbol{y},\boldsymbol{y}\middle|c_{n,j},\hat{\boldsymbol{h}}^{(i)}(t),\hat{\boldsymbol{h}}^{(i)}(t-1)\right)\\ &= v\tilde{\boldsymbol{H}}\tilde{\boldsymbol{H}}^{\mathrm{H}} + \left(v\sum_{k=0,k\neq n}^{N-1}\tilde{\boldsymbol{Z}}_k + \sigma_\omega^2\boldsymbol{I}_N\right) - v\tilde{\boldsymbol{h}}_n\tilde{\boldsymbol{h}}_n^{\mathrm{H}}\end{aligned} \tag{22}$$

where $\tilde{\boldsymbol{Z}}_k = \mathrm{Cov}\left(\boldsymbol{h}_k(t),\boldsymbol{h}_k(t)\middle|\hat{\boldsymbol{h}}^{(i)}(t),\hat{\boldsymbol{h}}^{(i)}(t-1)\right)$.

According to Eq. (7), the LLR λ_n of the QPSK-modulated symbol from the SISO equalizer can be written as

$$\lambda_n = 2\sqrt{2}\,\tilde{\boldsymbol{h}}_n^{\mathrm{H}}\tilde{\boldsymbol{\Sigma}}^{-1}\left(\boldsymbol{y} - \tilde{\boldsymbol{H}}\mathbb{E}^{(i)}(\boldsymbol{x}) + \tilde{\boldsymbol{h}}_n\mathbb{E}^{(i)}(x_n)\right) \tag{23}$$

Using the Woodbury matrix identity, we have

$$\lambda_n = \frac{2\sqrt{2}\,\tilde{\boldsymbol{h}}_n\boldsymbol{G}^{-1}}{1 - v\tilde{\boldsymbol{h}}_n^{\mathrm{H}}\boldsymbol{G}^{-1}\tilde{\boldsymbol{h}}_n}\left(\boldsymbol{y} - \tilde{\boldsymbol{H}}\mathbb{E}^{(i)}(\boldsymbol{x}) + \tilde{\boldsymbol{h}}_n\mathbb{E}^{(i)}(x_n)\right) \tag{24}$$

with $\boldsymbol{G} \triangleq v\tilde{\boldsymbol{H}}\tilde{\boldsymbol{H}}^{\mathrm{H}} + \left(v\sum_{k=0,k\neq n}^{N-1}\boldsymbol{Z}_k + \sigma_\omega^2\boldsymbol{I}_N\right)$. The LLRs $\lambda_{n,0}$ and $\lambda_{n,1}$ are the real and imaginary parts of λ_n, respectively.

3.2 Data-aided channel re-estimation

The LLR $\lambda_{n,j}$ is submitted into the SISO decoder to obtain the soft decision symbols $\mathbb{E}^{(i)}(\boldsymbol{x})$, which can be used to re-estimate the UWA channels $\boldsymbol{h}(t-1)$ and $\boldsymbol{h}(t)$. We have

$$\hat{\boldsymbol{h}}^{(i)}(t-1) = \boldsymbol{h}(t-1) + \left(\boldsymbol{S}^{(i)}(t-1)\right)^{\dagger}\boldsymbol{w}^{(i)}(t-1) \tag{25}$$

$$\hat{\boldsymbol{h}}^{(i)}(t) = \boldsymbol{h}(t) + \left(\boldsymbol{S}^{(i)}(t)\right)^{\dagger}\boldsymbol{w}^{(i)}(t) \tag{26}$$

where

$$\boldsymbol{S}^{(i)}(t-1) = \begin{bmatrix} s_{L-1} & s_{L-2} & \cdots & s_0\\ \vdots & & & \vdots\\ s_{P-1} & s_{P-2} & \cdots & s_{P-L}\\ \mathbb{E}^{(i)}(x_0) & s_{P-1} & \cdots & s_{P-L+1}\\ \vdots & & & \vdots\\ \mathbb{E}^{(i)}(x_{N-1}) & \mathbb{E}^{(i)}(x_{N-2}) & \cdots & \mathbb{E}^{(i)}(x_{N-L}) \end{bmatrix} \in \mathbb{C}^{(N+P-L+1)\times L} \tag{27}$$

$$\boldsymbol{S}^{(i)}(t) = \begin{bmatrix} \mathbb{E}^{(i)}(x_{L-1}) & \mathbb{E}^{(i)}(x_{L-2}) & \cdots & \mathbb{E}^{(i)}(x_0)\\ \vdots & & & \vdots\\ \mathbb{E}^{(i)}(x_{N-1}) & \mathbb{E}^{(i)}(x_{N-2}) & \cdots & \mathbb{E}^{(i)}(x_{N-L})\\ s_0 & \mathbb{E}^{(i)}(x_{N-1}) & \cdots & \mathbb{E}^{(i)}(x_{N-L+1})\\ \vdots & & & \vdots\\ s_{P-1} & s_{P-2} & \cdots & s_{P-L} \end{bmatrix} \in \mathbb{C}^{(N+P-L+1)\times L} \tag{28}$$

Similar to Zhu et al. (2016), we aim to enhance channel estimation by utilizing the CSI from the previous iteration. Then, we define

$$\boldsymbol{R}^{(i)}(t) \triangleq \boldsymbol{I}_L + \sigma_\omega^2(\boldsymbol{S}^{(i)}(t)^{\mathrm{H}}\boldsymbol{S}^{(i)}(t))^{-1} \tag{29}$$

and the re-estimated channels satisfy the distributions of $\hat{\boldsymbol{h}}^{(i)}(t)\sim\mathcal{CN}(\boldsymbol{0},\boldsymbol{R}^{(i)}(t))$ and $\hat{\boldsymbol{h}}^{(i-1)}(t)\sim\mathcal{CN}(\boldsymbol{0},\boldsymbol{R}^{(i-1)}(t))$. We combine the channels $\hat{\boldsymbol{h}}^{(i)}(t)$ and $\hat{\boldsymbol{h}}^{(i-1)}(t)$ to obtain a channel estimate $\hat{\boldsymbol{h}}^{B}(t)$ with minimum BMSE (Kay, 1993). It can be shown as

$$\hat{\boldsymbol{h}}^{B}(t) = \mathbb{E}_{\boldsymbol{h}(t),\boldsymbol{w}}\left(\boldsymbol{h}(t)\middle|\hat{\boldsymbol{h}}^{(i)}(t),\hat{\boldsymbol{h}}^{(i-1)}(t)\right) = \boldsymbol{J}(t)\begin{bmatrix}\hat{\boldsymbol{h}}^{(i)}(t)\\ \hat{\boldsymbol{h}}^{(i-1)}(t)\end{bmatrix} \tag{30}$$

where

$$\boldsymbol{J}(t) = \begin{bmatrix}\boldsymbol{I}_L & \boldsymbol{I}_L\end{bmatrix}\begin{bmatrix}\boldsymbol{R}^{(i)}(t) & \boldsymbol{I}_L\\ \boldsymbol{I}_L & \boldsymbol{R}^{(i-1)}(t)\end{bmatrix}^{-1} \tag{31}$$

3.3 *A posteriori* distribution update for the re-estimated channels

Autocorrection of the re-estimated channel $\hat{\boldsymbol{h}}^{B}(t)$ is

$$\begin{aligned}\boldsymbol{R}^{B}(t) &\triangleq \mathbb{E}_{\boldsymbol{h}(t)}\left(\hat{\boldsymbol{h}}^{B}(t)\hat{\boldsymbol{h}}^{B}(t)^{\mathrm{H}}\right)\\ &= \boldsymbol{J}(t)\begin{bmatrix}\boldsymbol{R}^{(i)}(t) & \boldsymbol{I}_L\\ \boldsymbol{I}_L & \boldsymbol{R}^{(i-1)}(t)\end{bmatrix}\boldsymbol{J}(t)^{\mathrm{H}}\\ &= \begin{bmatrix}\boldsymbol{I}_L & \boldsymbol{I}_L\end{bmatrix}\begin{bmatrix}\boldsymbol{R}^{(i)}(t) & \boldsymbol{I}_L\\ \boldsymbol{I}_L & \boldsymbol{R}^{(i-1)}(t)\end{bmatrix}^{-1}\begin{bmatrix}\boldsymbol{I}_L\\ \boldsymbol{I}_L\end{bmatrix}\end{aligned} \tag{32}$$

The cross-correlation of $\hat{\boldsymbol{h}}^{B}(t)$ and $\boldsymbol{h}(t)$ is given by

$$\mathbb{E}_{\boldsymbol{h}(t)}\left(\hat{\boldsymbol{h}}^{B}(t)\boldsymbol{h}(t)\right) = \boldsymbol{J}(t)\begin{bmatrix}\boldsymbol{I}_L\\ \boldsymbol{I}_L\end{bmatrix} = \boldsymbol{R}^{B}(t) \tag{33}$$

According to Eqs. (32) and (33), we can update the *a posteriori* distribution in Eq. (17) as

$$\left(\boldsymbol{h}(t)\,\middle|\,\hat{\boldsymbol{h}}^{B}(t),\hat{\boldsymbol{h}}^{B}(t-1)\right)\sim\boldsymbol{E}^{(i)}\boldsymbol{\zeta}^{(i)}(t)+\mathcal{CN}(\boldsymbol{0},\boldsymbol{Z}^{(i)}) \quad (34)$$

where

$$\boldsymbol{\zeta}^{(i)}(t)=\begin{bmatrix}\hat{\boldsymbol{h}}^{B}(t)\\ \hat{\boldsymbol{h}}^{B}(t-1)\end{bmatrix} \quad (35)$$

$$\boldsymbol{E}^{(i)}=\begin{bmatrix}\boldsymbol{R}^{B}(t) & \alpha\boldsymbol{R}^{B}(t)\end{bmatrix}\cdot\begin{bmatrix}\boldsymbol{R}^{B}(t) & \alpha\boldsymbol{R}^{B}(t-1)\\ \alpha\boldsymbol{R}^{B}(t-1) & \boldsymbol{R}^{B}(t-1)\end{bmatrix}^{-1} \quad (36)$$

$$\boldsymbol{Z}^{(i)}=\boldsymbol{I}_{L}-\boldsymbol{E}^{(i)}\begin{bmatrix}\boldsymbol{R}^{B}(t)\\ \alpha\boldsymbol{R}^{B}(t-1)\end{bmatrix} \quad (37)$$

The equalization coefficients in the next iteration can be updated by substituting Eq. (34) into Eq. (24). The values of $\boldsymbol{E}^{(0)}$, $\boldsymbol{\zeta}^{(0)}(t)$, and $\boldsymbol{Z}^{(0)}$ are obtained from Eq. (17), and $\mathbb{E}^{(0)}(\boldsymbol{x})$ is set to $\boldsymbol{0}$.

4 Simulation results

We validated the proposed algorithm through a Monte Carlo simulation, utilizing the UWA channels and passband signal measured from a hydrophone mounted on the bow of an autonomous underwater vehicle (AUV) during the experiment in Songhua Lake. The depth of the transmitting transducer was 15 m, and the receiving depth of the AUV was 3 m. The AUV maintained a speed of 3 kn and navigated a course that was perpendicular to the axis of the transmitting transducer. The transmitted frame consisted of five blocks, each with a data length of $N = 512$. Channel estimations were performed by the pilot sequences with a length of $P = 192$. The simulation used parameters including a bandwidth of $B = 4$ kHz, a center frequency of $f_c = 12$ kHz, and a sampling frequency of $f_s = 48$ kHz. The transmitted signal was encoded using a rate-1/2 convolutional code and modulated by QPSK. The duration of each frame was 3 s. Figures 3(a) and 3(b) show the pseudocolor map and coherence function of the UWA channels, respectively. We used root-mean-square delay (Bharadwaj and Koul, 2018) to measure the multipath propagation and channel coherence time (Tong et al., 2023) to measure the Doppler effect, which were approximately 20 ms and 0.7 s, respectively.

We used the turbo equalizer for channel equalization due to the complex multipath structure of the channel. We considered the following five schemes for comparison, which all used data-aided channel re-estimation to track the UWA channels.

• **Case I**: Conventional turbo equalization (Zheng et al., 2015) with LS channel estimation. We consider Case I as the benchmark.

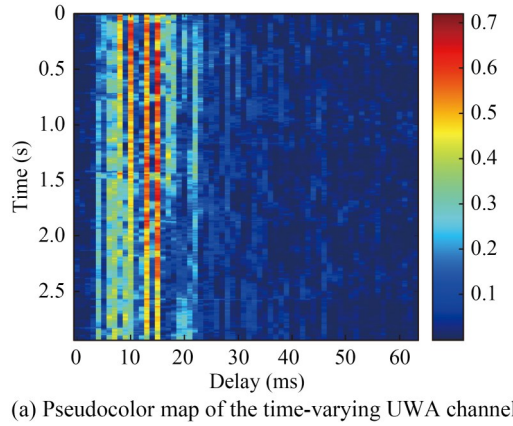

(a) Pseudocolor map of the time-varying UWA channels

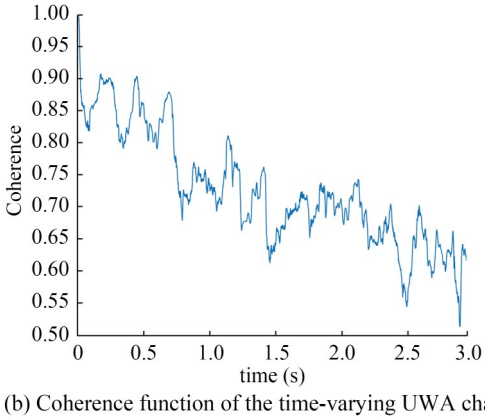

(b) Coherence function of the time-varying UWA channels

Figure 3 Measured UWA channels from the AUV experiment in Songhua Lake

• **Case II**: Conventional turbo equalization (Zheng et al., 2015) with SBL channel estimation.

• **Case III**: Turbo equalization with LS channel estimation and CEE compensation (Li et al., 2016).

• **Case IV**: Turbo equalization with BCE (Yang et al., 2021). The AR(1) factor is $\alpha = 1$.

• **Case V**: Proposed algorithm. The AR(1) factor is $\alpha = 1$.

Figure 4 compares the BER performance of the proposed algorithm (Case V) against those of the other four schemes with iterations of 0, 1, and 5. The performance of Case I is the worst in any iteration due to the CEEs caused by LSE and neglect of the sparsity of the UWA channel. Despite LS channel estimation, Case V still outperforms Case II. This superior performance can be attributed to the fact that the channel *a posteriori* distribution realized by the AR process and the imperfect CSI provide a higher channel estimation accuracy than SBL channel estimation. The reason for the BER performance gap between Case III and Case V is that Case III does not consider the channel $\boldsymbol{h}(t-1)$ at the previous moment. Due to the time-varying nature of the channel, the algorithms that consider the AR(1) process, namely Case IV and Case V, perform better than the algorithms that assume that the channel is time-invariant within a block. Although Case IV uses forward and backward AR processes, its BER is higher than that of Case V. For exam-

ple, at an SNR of 8 dB, the BER of Case V is 6.6×10^{-4} in the fifth iteration, while that of Case IV is 4.3×10^{-3}. This is because Case V considers the imperfect CSI at moments t and $(t-1)$, resulting in a more accurate channel *a posteriori* distribution.

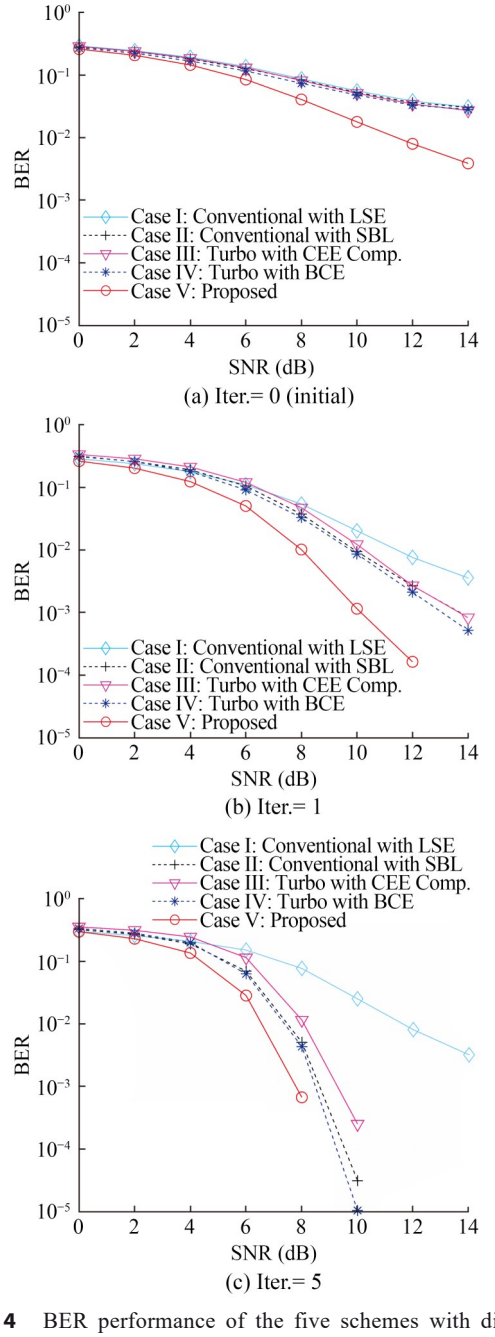

Figure 4 BER performance of the five schemes with different iterations

Figure 5 shows the BER performance of BCE-Turbo (Case IV) and the proposed algorithm under different AR(1) factors α in the fifth iteration. The proposed algorithm outperforms BCE-Turbo under any value of α. Moreover, the performance of the proposed algorithm is relatively robust as its BER performance exhibits a minimal variation with changes in α. For example, at a BER of 10^{-3}, the maximum gain difference for the proposed algorithm is 0.014 dB, while that for BCE-Turbo is 0.346 dB. Therefore, the proposed algorithm is not sensitive to the selection of α.

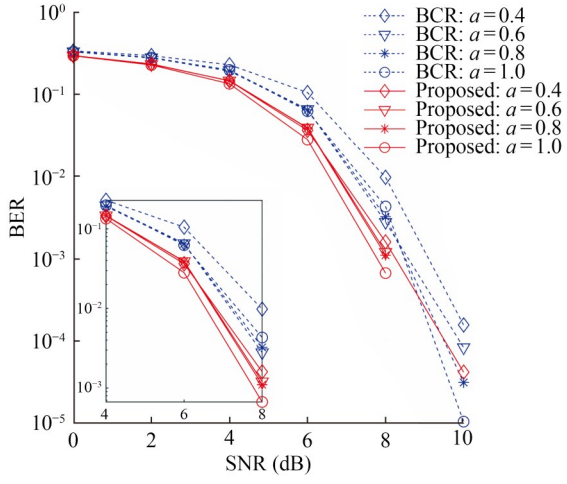

Figure 5 BER performance under different α values in the fifth iteration

5 Computational complexity analysis

We use the method of calculating the floating-point operations (flops) per iteration to assess the computational complexity (Yin et al., 2024). Each flop represents a real addition or multiplication, among other operations. Specifically, a complex addition involves two flops, while a complex multiplication requires six flops. We focus on the computational complexity of the algorithms with similar structures, such as Case I, Case III, and Case V.

5.1 SISO equalization

For Case I, the computational complexity primarily arises from calculating $\boldsymbol{\Sigma}$ and its inverse matrix during SISO equalization. The complexity of computing $\boldsymbol{\Sigma}$ mainly exists in calculating $\boldsymbol{H}\boldsymbol{H}^{\mathrm{H}}$. For the nondiagonal elements of $\boldsymbol{H}\boldsymbol{H}^{\mathrm{H}}$, it requires $N^2(N-1)$ complex additions and multiplications, thus needing $N^2(N-1)$ flops. In contrast, for its diagonal elements, because the multiplied elements are conjugates, only $4N^2$ flops are needed. Computing $\boldsymbol{\Sigma}^{-1}$ requires $4N^3$ flops.

The difference in SISO equalization between Case I and Case III mainly exists in the composition of the channel matrix $\boldsymbol{H}$, but the overall computational complexity remains the same (Li et al., 2016). Case V involves additional computations of $v\sum_{k=0,k\neq n}^{N-1}\tilde{\boldsymbol{Z}}_k$ compared to Case I, which requires N^2 flops because $\tilde{\boldsymbol{Z}}_k$ is a real matrix.

5.2 Initial channel estimation

In the initial iteration of Case I, the computational com-

plexity of the LS channel estimation primarily lies in calculating the pseudoinverse of the matrix $\boldsymbol{S}$, requiring $16L^2P - 4PL - 12L^3 + 20L^2 - 4L$ flops. On the basis of LSE, Case III also utilizes the estimated channel to compute the channel *a posteriori* distribution $p\left(\boldsymbol{h}(t)\middle|\hat{\boldsymbol{h}}(t)\right)$, where the main computational complexity exists in calculating $\boldsymbol{R}$, needing $8PL^2 + 12L^2 - 4PL - 3L$ flops. Furthermore, computing the channel *a posteriori* distribution $p\left(\boldsymbol{h}(t)\middle|\hat{\boldsymbol{h}}(t),\hat{\boldsymbol{h}}(t-1)\right)$ requires $8PL^2 + 40L^3 + 20L^2 - 4PL - 3L$ flops, as Case V considers the channel from the previous moment.

5.3 Channel update

When using the soft information output from the SISO decoder for channel updating, Cases I and III require only one LSE, and the order of magnitude of flops for calculating $\left(\boldsymbol{S}^{(i)}(t)\right)^{\dagger}$ changes to $\mathcal{O}\left(NL^2 + PL^3 + L^3\right)$, while Case V requires two LSEs. Additionally, in Case V, the complexity of calculating $\hat{\boldsymbol{h}}^B(t)$ primarily resides in computing $\boldsymbol{R}^{(i)}(t)$, with the order of magnitude of flops also being $\mathcal{O}\left(NL^2 + PL^3 + L^3\right)$. When updating the channel *a posteriori* distribution, computing $\boldsymbol{R}^B(t)$ requires $12L^3$ flops, and the number of flops for calculating the channel *a posteriori* mean and variance remains the same as in the initial channel estimation.

Table 1 shows the final computational complexity of Cases I, III, and V. Figure 6 illustrates the relationship between the flops, block length N, pilot sequence length P, and channel length L. The black circles in the diagram indicate the number of flops required under the parameter settings in Section 4. From the diagram, it is evident that the performance improvement of Case V over Case I and Case III comes at the cost of increased computational complexity. Nevertheless, the computational complexity of the three schemes is of the same order of magnitude. Therefore, the increase in computational complexity caused by the proposed algorithm is acceptable.

Table 1 Computational complexity of Cases I, III, and V

Algorithm	SISO equalization (flops)	Initial channel estimation (flops)	Channel update (flops)
Case I	$M\,(12N^3 + 21N^2 + 13N + 2M + 4)$	$16PL^2 - 12L^3 + 4PL + 12L^2 + 4L$	$16NL^2 + 16PL^2 - 12L^3 + 12L^2 + 4NL + 4PL + 4L$
Case III	$M\,(12N^3 + 21N^2 + 13N + 2M + 4)$	$24PL^2 - 12L^3 + 32L^2 + 2L$	$24NL^2 + 24PL^2 + 4L^3 + 42L^2 - 12NL - 12PL - 8L$
Case V	$M\,(12N^3 + 22N^2 + 13N + 2M + 4)$	$40PL^2 + 16L^3 + 4PL + 44L^2 + 5L$	$64NL^2 + 64PL^2 + 40L^3 + 96L^2 - 8NL - 8PL - 3L$

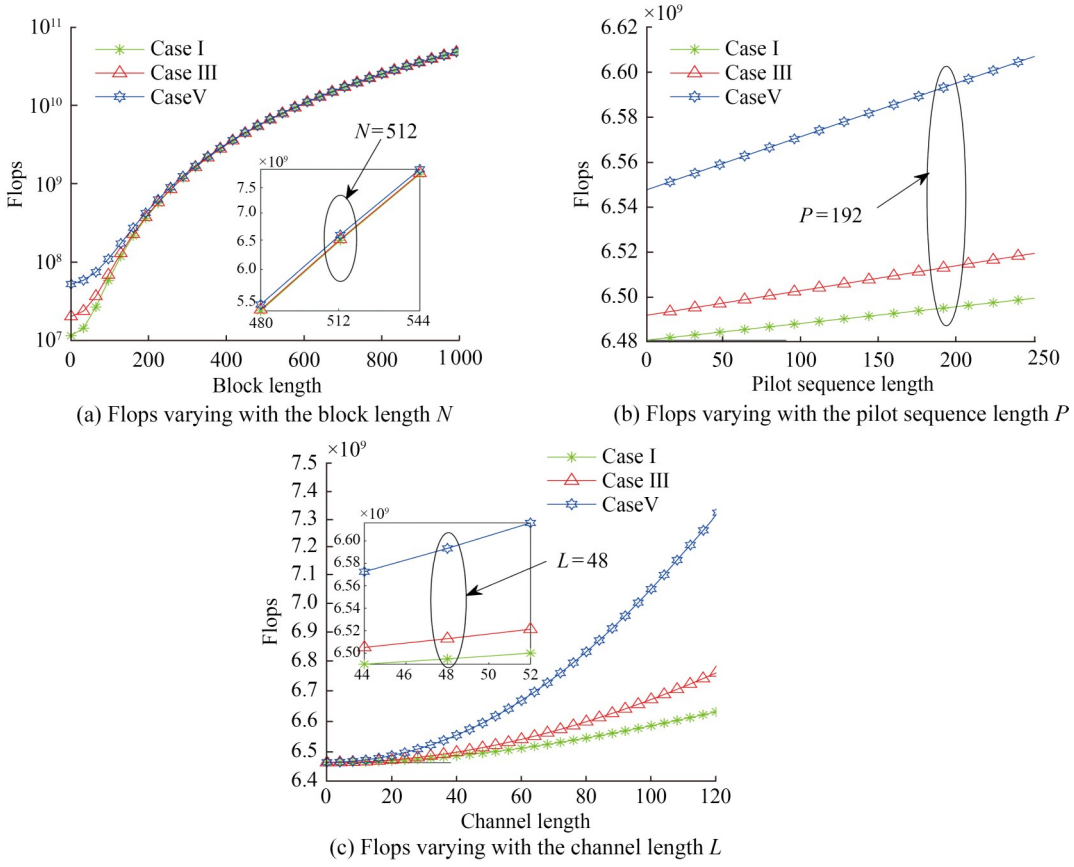

(a) Flops varying with the block length N

(b) Flops varying with the pilot sequence length P

(c) Flops varying with the channel length L

Figure 6 Relationship between the flops, block length, pilot sequence length, and channel length

6 Conclusions

A turbo equalization algorithm for time-varying UWA channels was proposed. First, we derived the turbo equalizer based on the JG criterion. Subsequently, by leveraging imperfect CSI combined with an AR(1) model, a more precise channel *a posteriori* distribution is obtained. The distribution is subsequently utilized in the design of the turbo equalizer, performing a more effective mitigation of the multipath propagation and Doppler effect in UWA channels. Simulation results show that: 1) the BER of the proposed algorithm is at least one order of magnitude lower than those of other methods when the SNR exceeds 8 dB after five iterations during the AUV mobile communication. 2) the proposed algorithm has a robust performance with changes in the AR(1) factor, while the performance of the comparison method using AR process will significantly change. 3) The proposed algorithm has increased the acceptable computational complexity compared to other methods.

Funding Supported by the National Natural Science Foundation of China (Grant No. 62301181), and the Excellent Youth Science Fund of Heilongjiang Province (Grant No. YQ2022F001).

Competing interest Wei Ge is an editorial board member for the Journal of Marine Science and Application and was not involved in the editorial review, or the decision to publish this article. All authors declare that there are no other competing interests.

References

Abdelkareem AE, Sharif BS, Tsimenidis CC, Neasham JA, Hinton OR (2011) Low-complexity Doppler compensation for OFDM-based underwater acoustic communication systems. OCEANS 2011 IEEE-Spain, Santander, Spain, 1-6

Abdelkareem AE, Sharif BS, Tsimenidis CC (2016) Adaptive time varying Doppler shift compensation algorithm for OFDM-based underwater acoustic communication systems. Ad Hoc Networks 45: 104-119. https://doi.org/10.1016/j.adhoc.2015.05.011

Bharadwaj R, Koul SK (2018) Experimental analysis of ultra-wideband body-to-body communication channel characterization in an indoor environment. IEEE Transactions on Antennas and Propagation 67(3): 1779-1789. https://doi.org/10.1109/TAP.2018.2883634

Fodor G, Fodor S, Telek M (2021) Performance analysis of a linear MMSE receiver in time-variant Rayleigh fading channels. IEEE Transactions on Communications 69(6): 4098-4112. https://doi.org/10.1109/TCOMM.2021.3061680

Fodor S, Fodor G, Gürgünoğlu D, Telek M (2023) Optimizing pilot spacing in MU-MIMO systems operating over aging channels. IEEE Transactions on Communications 71(6): 3708-3720. https://doi.org/10.1109/TCOMM.2023.3261384

Ge W, Wang Z, Yin J, Han X (2024) Robust equalization for single-carrier underwater acoustic communications based on parameterized interference model. IEEE Wireless Communications Letters 13(9): 2312-2316. https://doi.org/10.1109/LWC.2022.3223533

Guo Q, Ping L, Huang D (2009) A low-complexity iterative channel estimation and detection technique for doubly selective channels. IEEE Transactions on Wireless Communications 8(8): 4340-4349. https://doi.org/10.1109/TWC.2009.081448

Guo Z, Song A, Towliat M, Cimini L, Xia X (2021) Impacts of channel fluctuations on least-squares channel estimation in underwater acoustic communications. The Journal of the Acoustical Society of America 149(6): 3929-3942. https://doi.org/10.1121/10.0005087

Jiang F, Li C, Gong Z (2018) Accurate analytical BER performance for ZF receivers under imperfect channel in low-SNR region for large receiving antennas. IEEE Signal Processing Letters 25(8): 1246-1250. https://doi.org/10.1109/LSP.2018.2849683

Jiang W, Diamant R (2023) Long-range underwater acoustic channel estimation. IEEE Transactions on Wireless Communications 22(9): 6267-6282. https://doi.org/10.1109/TWC.2023.3241230

Kay S (1993) Statistical signal processing: estimation theory. Prentice Hall, New York, 225-226

Khan M, Das B, Pati B (2020) Channel estimation strategies for underwater acoustic (UWA) communication: An overview. Journal of the Franklin Institute 357(11): 7229-7265. https://doi.org/10.1016/j.jfranklin.2020.04.002

Li C, Jiang F, Meng C, Gong Z (2016) A new turbo equalizer conditioned on estimated channel for MIMO MMSE receiver. IEEE Communications Letters 21(4): 957-960. https://doi.org/10.1109/LCOMM.2016.2638823

Liang Y, Yu H, Ji F, Chen F (2023) Multitask sparse Bayesian channel estimation for turbo equalization in underwater acoustic communications. IEEE Journal of Oceanic Engineering 48(3): 946-962. https://doi.org/10.1109/JOE.2022.3229902

Liu Y, Zhao Y, Gerstoft P, Zhou F, Qiao G, Yin J (2023) Deep transfer learning-based variable Doppler underwater acoustic communications. The Journal of the Acoustical Society of America 154(1): 232-244. https://doi.org/10.1121/10.0020147

Naman HA, Abdelkareem AE (2023) Multipath geometry channel model in shallow water acoustic communication. Journal of Marine Science and Application 22(2): 359-369. https://doi.org/10.1007/s11804-023-00339-5

Roudsari HM, Bousquet JF, McIntyre G (2017) Channel model for wideband time-varying underwater acoustic systems. OCEANS 2017-Aberdeen, Aberdeen, UK, 1-7

Sun D, Wu J, Hong X, Liu C, Cui H, Si B (2023) Iterative double-differential direct-sequence spread spectrum reception in underwater acoustic channel with time-varying Doppler shifts. The Journal of the Acoustical Society of America 153(2): 1027-1041. https://doi.org/10.1121/10.0017116

Tao J (2015) Single-carrier frequency-domain turbo equalization with various soft interference cancellation schemes for MIMO systems. IEEE Transactions on Communications 63(9): 3206-3217. https://doi.org/10.1109/TCOMM.2015.2459054

Tong W, Ge W, Han X, Yin J (2023) An iterative subblock-based receiver for SC-FDE systems in time-varying underwater acoustic channels. Applied Acoustics 211: 109566. https://doi.org/10.1016/j.apacoust.2023.109566

Tüchler M, Singer AC, Koetter R (2002) Minimum mean squared error equalization using a priori information. IEEE Transactions on Signal Processing 50(3): 673-683. https://doi.org/10.1109/78.984761

Yang G, Guo Q, Ding H, Yan Q, Huang D (2021) Joint message-passing-based bidirectional channel estimation and equalization with superimposed training for underwater acoustic communications. IEEE Journal of Oceanic Engineering 46(4): 1463-1476. https://doi.org/10.1109/JOE.2021.3057916

Yang G, Guo Q, Qin Z, Huang D, Yan Q (2022) Belief-propagation-based low-complexity channel estimation and detection for underwater acoustic communications with moving transceivers.

IEEE Journal of Oceanic Engineering 47(4): 1246-1263. https://doi.org/10.1109/JOE.2022.3148567

Yin J, Ge W, Han X, Liu B, Guo L (2019) Partial FFT demodulation with IRC in MIMO-SC-FDE communication over Doppler distorted underwater acoustic channels. IEEE Communications Letters 23(11): 2086-2090. https://doi.org/10.1109/LCOMM.2019.2937860

Yin J, Zhu G, Han X, Guo L, Li L, Ge W (2024) Temporal correlation and message-passing-based sparse Bayesian learning channel estimation for underwater acoustic communications. IEEE Journal of Oceanic Engineering 49(2): 522-541. https://doi.org/10.1109/JOE.2023.3330523

Yuan X, Guo Q, Wang X, Ping L (2008) Evolution analysis of low-cost iterative equalization in coded linear systems with cyclic prefixes. IEEE Journal on Selected Areas in Communications 26(2): 301-310. https://doi.org/10.1109/JSAC.2008.080207

Zhang M, Zhu J, Wang Y, Fu Y, Wei Y, Tu X, Qu F (2024) Joint channel estimation, data decoding and group-sparse impulsive noise estimation for slowly time-varying single carrier underwater acoustic communications. IEEE Access 12: 40139-40152. https://doi.org/10.1109/ACCESS.2024.3374118

Zhang Y, Venkatesan R, Dobre OA, Li C (2019) Efficient estimation and prediction for sparse time-varying underwater acoustic channels. IEEE Journal of Oceanic Engineering 45(3): 1112-1125. https://doi.org/10.1109/JOE.2019.2911446

Zhang Y, Wang H, Li C, Chen X, Meriaudeau F (2022) On the performance of deep neural network aided channel estimation for underwater acoustic OFDM communications. Ocean Engineering 259: 111518. https://doi.org/10.1016/j.oceaneng.2022.111518

Zhang Y, Zakharov Y, Li J (2018) Soft-decision-driven sparse channel estimation and turbo equalization for MIMO underwater acoustic communications. IEEE Access 6: 4955-4973. https://doi.org/10.1109/ACCESS.2018.2794455

Zhe P, Zhu Y, Letaief K (2018) Robust single-carrier frequency-domain equalization for broadband MIMO systems with imperfect channel estimation. IEEE Transactions on Wireless Communications 17(7): 4432-4446. https://doi.org/10.1109/TWC.2018.2825340

Zheng YR, Wu J, Xiao C (2015) Turbo equalization for single-carrier underwater acoustic communications. IEEE Communications Magazine 53(11): 79-87. https://doi.org/10.1109/MCOM.2015.7321975

Zhu Y, Zhe P, Zhou H, Huang D (2016) Robust single carrier frequency domain equalization with imperfect channel knowledge. IEEE Transactions on Wireless Communications 15(9): 6091-6103. https://doi.org/10.1109/TWC.2016.2578332